RESEARCH ARTICLE OPEN ACCESS

Spatial–Temporal Variability of Hourly Precipitation Extremes in Portugal: Two Case Studies in Major Wine-Growing Regions

José Cruz[1] | Margarida Belo-Pereira[2] | André Fonseca[1] | João A. Santos[1]

[1]Institute for Innovation, Capacity Building and Sustainability of Agri-Food Production (Inov4Agro), Centre for the Research and Technology of Agro-Environmental and Biological Sciences (CITAB), Universidade de Trás-Os-Montes e Alto Douro (UTAD), Vila Real, Portugal | [2]Instituto Português do Mar e da Atmosfera, Divisão de Meteorologia Aeronáutica, Lisboa, Portugal

Correspondence: José Cruz (josecruz@utad.pt)

ABSTRACT

Heavy precipitation events are a natural hazard that have significant socioeconomic implications, especially in sectors like agriculture, namely viticulture. This study is the first to present a detailed climatology of extreme precipitation across mainland Portugal, leveraging hourly data gathered from 71 meteorological stations over 23 years, spanning from 2000 to 2022. To understand spatial variability, we focus on Douro and Alentejo, two major winemaking regions where extreme weather events may have significant adverse consequences. High spatial variability in the β-index patterns (mean ratio between over-threshold precipitation and total precipitation) shows that hourly precipitation between 10 and 20 mm h^{-1} contributes the most to winter and autumn precipitation, whereas events exceeding 20 mm h^{-1} play a more significant role in summer and autumn. Extreme events occur most frequently between September and December, with a secondary peak observed in April and May, particularly pronounced in Alentejo. The diurnal cycle, which displays a peak in the afternoon, exhibits a close relationship with the occurrence of thunderstorms. A more in-depth analysis was conducted to examine the dynamic and thermodynamic mechanisms that contributed to two extreme precipitation events caused by thunderstorms in the Douro and Alentejo winemaking regions. Differing synoptic environments led to unstable conditions at the origin of these events. The Douro event was driven by a cut-off low, whereas the Alentejo event was related to an extratropical cyclone, both in their final stages of development. The regional indices and seasonal patterns identified offer insights into spatial distribution and seasonality, essential for future research and applied climate adaptation strategies.

1 | Introduction

The Iberian Peninsula (IP), owing to its location in South–western Europe, between the subtropical high-pressure belt and the mid-latitude eddy-driven westerly jet stream and to its complex terrain features (e.g., several mountain ranges with inner sheltered plateaus), is a challenging region for the analysis of precipitation variability (Casado et al. 2010; Ramos, Cortesi, and Trigo 2014). Different studies carried out on monthly and daily timescales (Belo-Pereira et al. 2011; Cardoso et al. 2013; Ramos, Trigo, and Liberato 2014; Ramos et al. 2018) revealed pronounced seasonal precipitation regimes and accentuated

spatial gradients in IP, because of its orography, the influence of the ocean, and the diverse patterns of atmospheric circulation (Mills 1995; Esteban-Parra et al. 1998; Rodriguez-Puebla et al. 1998; Trıgo and Da Câmara 2000; Nieto et al. 2007; Santos et al. 2007). Heavy precipitation events in the IP are usually associated with the presence of intense extratropical cyclones (Trigo 2006; Hawcroft et al. 2012; Liberato 2014; Liberato and Trigo 2014; Santos and Belo-Pereira 2022), which are more common from October to December. Extreme precipitation events may also be associated with squall lines favoured by upper-cold fronts (Pinto and Belo-Pereira 2020), or by mesoscale convective systems, originating in the Mediterranean Sea, under the presence of cut-off lows (Cohuet et al. 2011).

In particular, in mainland Portugal, located on the Atlantic-facing side of the IP, precipitation is highly concentrated in the autumn and winter months (Santos et al. 2005), mostly favoured by westerly/south–westerly air flows and embedded travelling cyclones developing over the North Atlantic (Trıgo and Da Câmara 2000; Santos et al. 2005). The intra- and inter-annual variability of precipitation in Portugal is strongly linked to the variability of large-scale eddies (Santos, Andrade, et al. 2009; Santos, Pinto, and Ulbrich 2009; Ramos et al. 2015), connected to jet stream wave-breaking episodes (Woollings et al. 2011; Santos et al. 2013). Atmospheric rivers have been related to precipitation extremes in Portugal (Ramos et al. 2015, 2018). In mainland Portugal, convective precipitation depicts a bimodal distribution (Santos and Belo-Pereira 2019), with maxima in April and October, though more pronounced in the latter and over the inner areas of the country (more continental climates). Moreover, the previous studies hinted at the strong spatial gradients of precipitation and its extremes over mainland Portugal, as well as the different temporal regimes, thereby justifying the selection of different locations in the country to be representative of this spatial and temporal variability. This variability was studied by Fonseca et al. (2023), using 17 climate extreme indices for Portugal's designated wine denomination regions and subregions. The study of precipitation variability is essential for viticulture, as water stress affects vine growth at its various developmental stages (Austin and Bondari 1988). Adequate moisture is crucial at the start of development for good growth and the formation of flowers and berries, whereas excess water at this stage can increase foliage density and the risk of disease. Between flowering and berry ripening, moderately dry conditions favour wine quality, as severe water stress can reduce leaf area and cause flowers and clusters to drop (Hardie and Martin 2000; Paranychianakis et al. 2004; Fraga et al. 2012).

To understand and evaluate the spatial–temporal variability of precipitation, heavy precipitation indices are widely used, commonly based on the daily precipitation (Jones et al. 1999; Karl et al. 1999; Brunetti et al. 2001). However, due to the frequent lack of dense weather station (WS) networks over large areas, most studies on heavy precipitation indices rely on time series analysis for specific locations rather than analysing spatial–temporal patterns (Kostopoulou and Jones 2005; Moberg and Jones 2005; Rodrigo and Trigo 2007; Costa and Soares 2008). Recently, Llasat et al. (2021) analysed the distribution and temporal evolution of convective precipitation in the Mediterranean region of Spain using the β-index. They defined the ratio of

convective precipitation to total precipitation, with an average 5-min intensity threshold of $35\,\mathrm{mm\,h^{-1}}$. Llasat et al. (2021) showed that convective precipitation can contribute, on average, up to 16% of the total annual precipitation, with summer being the most convective season. A similar approach is proposed in the present work, which involves calculating various heavy precipitation indices to analyse the spatio-temporal distribution of extreme precipitation events in mainland Portugal. These indices are derived from hourly precipitation totals, computed from 10-min observations, to allow for a standardised analysis of precipitation intensity. This analysis is carried out across different seasons using various precipitation thresholds, according to the warning criteria set by the Portuguese Weather Service (*Instituto Português do Mar e da Atmosfera*—IPMA—https://www.ipma.pt/en/index.html).

Although climate projections reveal an overall decrease in total precipitation in the IP, an increase in heavy precipitation events, in terms of both frequency and intensity, accompanied by a significant increase in dry spell lengths, is expected over wide areas of the IP (Cardoso et al. 2019; Lee et al. 2023). The persistent and recurring dry spells reduce soil moisture, favouring soil degradation and desertification, making the IP increasingly susceptible to heavy precipitation events, soil erosion and loss (Pachauri et al. 2014; Lee et al. 2023). The occurrence of flooding in the Mediterranean region is indeed strongly connected to these extreme events (Cortès et al. 2018). The study of heavy precipitation events on a regional basis is of paramount importance for various purposes, such as for planning and forecasting floods (Prata Gomes et al. 2016), landslides (Moreno et al. 2024), soil erosion (Prachowski et al. 2024) and socioeconomic impacts (Frame et al. 2020). The present study is focused on the winemaking sector in Portugal because of its socioeconomic relevance and high susceptibility to extreme precipitation events. The increase in extreme precipitation events, accompanied by an increase in prolonged droughts, makes the winemaking sector particularly vulnerable (Santos et al. 2020; Straffelini and Tarolli 2023), especially in regions characterised by steep slopes (Wang et al. 2022). Such events can lead to severe soil erosion and loss, landslides, or even the collapse of vineyard terraces, among many other damages to infrastructures (Santos et al. 2015). They may also lead to increased disease prevalence and higher production costs while reducing grapevine yields (Sanderson et al. 2023).

Therefore, the present study aims to: (1) Characterise the spatial–temporal distribution of heavy precipitation events throughout Portugal and (2) develop a climatology of these events based on 10-min observations from surface WSs for the period 2000–2022 (23 years). These data will allow us to characterise the risk of extreme events for different regions, namely in wine regions, which are exposed and particularly vulnerable to their occurrence. They can also be used as an example of the applicability of this research, as a better understanding of these events can support decision-making and represent an important added value to a major socioeconomic sector in Portugal. In summary, the analysis is illustratively applied to two wine-growing regions in Portugal, with different climatic conditions, one in the north (Douro) and one in the south (Alentejo), though this method can be easily replicated for any other regions. The third objective of this study

is to analyse two heavy precipitation events, one from each targeted region as case studies, to diagnose and elucidate their dynamic and thermodynamic drivers. These two extreme events were selected in close collaboration with two winemaking companies, of which one is based in the Douro/Port wine region (Quinta do Bomfim—Symington Family Estates) and the other in the Alentejo wine region (Herdade do Esporão). The severity of these events, as well as the damage they caused in the vineyards, were taken into account. These events serve not only as case studies of heavy precipitation but also as examples for understanding the specific weather conditions and atmospheric dynamics associated with such severe weather patterns. This knowledge can be used to improve the performance of IPMA's weather forecasting system. Section 2 will describe the datasets and applied methodologies, whereas the results will be presented in Section 3. A discussion of the outcomes and main conclusions will be drawn in Section 4.

2 | Data and Methods

2.1 | Observational Data

This study uses observations from 71 WSs distributed over mainland Portugal, covering 23 years from January 2000 to December 2022, with a 10-min temporal resolution. The complete list of WSs is provided in Table S1, along with their

codes, designations, geographical coordinates (latitude and longitude) and elevation. The geographical distribution of the WSs throughout Portugal shows a relatively high density and uniformity, with fairly good coverage of the territory, a particularly important factor given that the elevation varies significantly between the northern region, with complex orography, and the southern region, characterised by lowland or smooth hilly areas (Figure 1).

The WSs, maintained by the Portuguese Weather Service (IPMA), provide 10-min observations of different atmospheric variables, including total precipitation (mm), air temperature (°C), mean sea level pressure (hPa), relative humidity (%), wind speed (m s^{-1}) and direction (°), as well as wind gust (m s^{-1}) and gust direction (°). Preliminary data quality analysis, isolation of inhomogeneities, and the removal of erroneous or inconsistent values are routinely carried out by IPMA (Santos and Belo-Pereira 2022). Since the automatic WSs were installed in different years, some of them present significant data gaps for the selected period (2000–2022), that is, the measured records of the WSs are frequently shorter than the full reference period.

To obtain the most complete precipitation time series possible, thus minimising the percentage of missing values, data from the closest stations (< 5 km in flat-terrain areas) were grouped into a single time series (station clusters), considering the
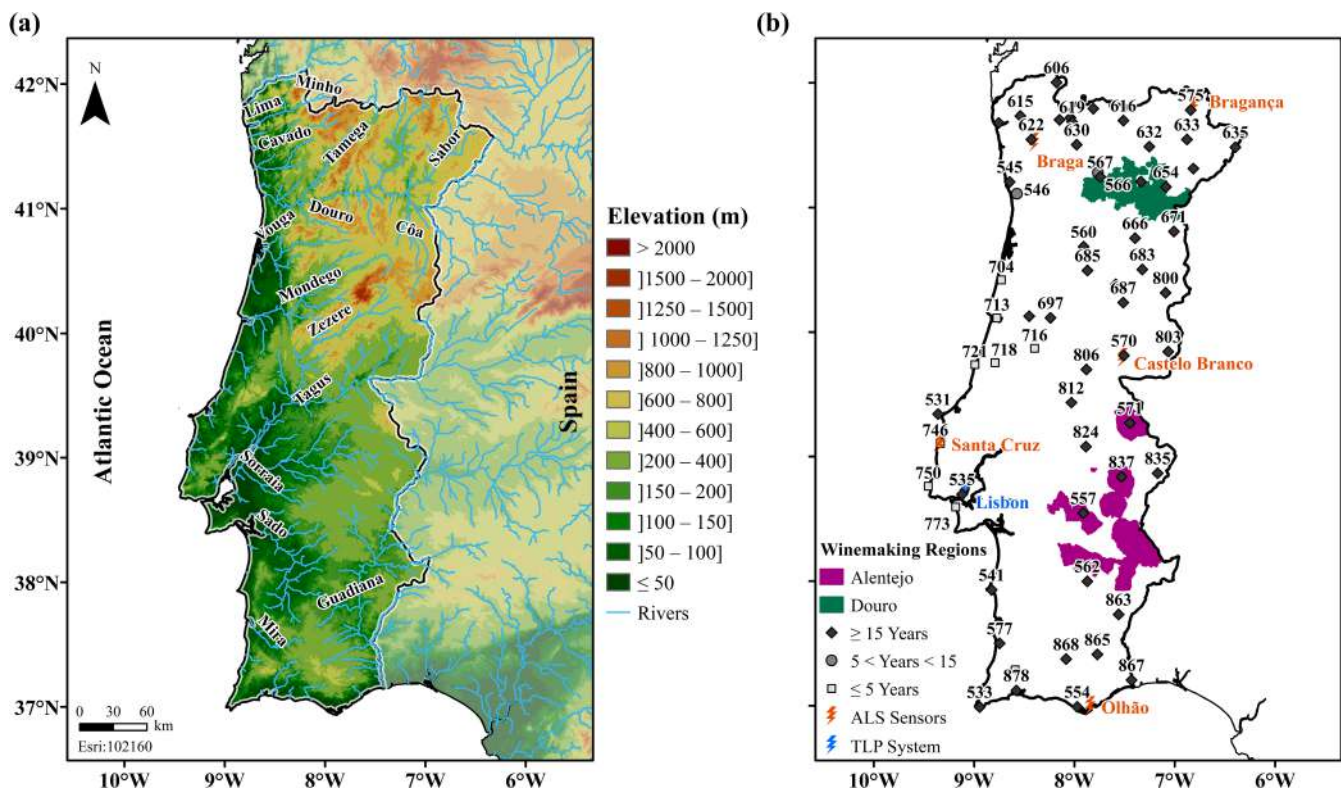
FIGURE 1 | (a) Hypsometric chart of mainland Portugal (elevation in meters), with the blue lines representing the major rivers. (b) Representation of the two major winemaking regions, located in the northern region (Douro—represented in green) and south-central area (Alentejo—represented in magenta) and spatial distribution of the surface weather stations in mainland Portugal. Light grey squares identify surface weather stations with equal or less than 5 years of data. Grey circles and dark grey diamonds represent surface weather stations with data between 6 and 14 years and equal or more than 15 years, respectively. Spatial distribution of five Advanced Lightning Sensors (LS7002) (represented in orange) and of the TLP (total lightning processor) system (represented in blue).

following criteria: (i) A missing value is considered when none of the stations in the same cluster present data (missing data are not replaced but are instead discarded from the analysis), (ii) if only one of the stations in a given cluster has a precipitation observation, this is the value considered, and, finally, (iii) if several stations in a given cluster present precipitation data, the maximum recorded value is eventually considered. After clustering the stations, a network of 63 observation sites was achieved (Figure 1b). All information on the WS, as well as the corresponding percentages of missing data on the 10-min timescale, are shown in Table S1.

After assessing the amount of missing data for each WS, the quality of the precipitation series from the 63 WS was also evaluated. Following the methodology described by (Santos and Fragoso 2013), potential inhomogeneities were identified using the number of wet days, defined as days with precipitation exceeding 1 mm. This metric tends to show lower variability than annual precipitation totals, particularly in regions with a high contribution from convective precipitation.

As proposed by (Santos and Fragoso 2013), for the analysis, four absolute homogeneity tests were applied using XLSTAT software, all with a 5% significance level: the Pettitt test (Pettit 1979), the SNHT—standard normal homogeneity test (Alexandersson 1986), the Buishand test (Buishand 1982) and the Von Neumann test (Von Neumann 1941). The final classification of series quality was designated as 'useful' when the series was considered homogeneous by all tests; 'potentially useful' when the series failed only one test but remained homogeneous in the others; and 'rejected' when two or more tests indicated inhomogeneity. Initially, the rejected series were re-evaluated by checking for the presence of linear trends, which were subsequently removed as they may be related to physically meaningful climate change trends rather than to inhomogeneities in the time series. The homogeneity tests were applied again to the new time series.

The results of the homogeneity assessment are presented in Table S2, where 44 series were classified as 'useful' and 9 as 'potentially useful', failing only one of the tests. Ten series were not tested because their sampling period was less than 10 years. However, the absence of these tests does not impact the main results, as the objective is the identification of extreme precipitation events, not the analysis of trends.

Lastly, data on atmospheric electrical discharges (AED) were also analysed. In mainland Portugal, the Network for the detection and localisation of AED, operated by IPMA, is currently composed of five Advanced Lightning Sensors LS7002 (Vaisala 2024a), installed in Bragança, Braga, Castelo Branco, Santa Cruz and Olhão (Figure 1b and Table S3). A TLP (total lightning processor) system (Vaisala 2024b) has been installed at the IPMA headquarters in Lisbon. The detection and localisation process also benefits from AEMET's network (with 6 sensors near the Portuguese–Spanish border). This system has a detection efficiency greater than 90% for cloud-to-ground discharges and 50% for intra-cloud electrical discharges (Vaisala 2024b) and a location accuracy of 250 to 1000 m, with decreasing accuracy from north–east to south–west in mainland Portugal (Schulz et al. 2016).

2.2 | Hourly Precipitation Events

For the spatial–temporal characterisation of the precipitation events in Portugal, hourly precipitation totals were calculated for the selected meteorological stations. These values were obtained by summing 10-min amounts and were discarded when a missing value occurred in the period. Using hourly data facilitates the application of the different thresholds considered in the criteria for issuing weather warnings by IPMA (IPMA 2024). As such, hourly precipitation was defined in the following classes: $10 \leq I < 20\,\mathrm{mm\,h^{-1}}$ (yellow warnings [YWs]) and $I \geq 20\,\mathrm{mm\,h^{-1}}$ (orange–red warnings [ORW]). A comparison with the hourly precipitation percentiles for all hours with $I \geq 0.1\,\mathrm{mm\,h^{-1}}$ revealed that the 95th percentile varies approximately from 2 to 6 mm h^{-1}, whereas the 99th percentile ranges from 6 to 12 mm h^{-1}. The 99.5th percentile varies between 7 and 16 mm h^{-1} and the 99.9th percentile varies between 9 and 35 mm h^{-1}, values closer to the ORWs (Table S2). Therefore, the selected events herein correspond to precipitation intensities above the 99th percentile, thus highlighting their exceptionality. Furthermore, the use of percentile-based thresholds makes comparing stations and regions difficult to assess, as the precipitation intensities corresponding to the same percentile can vary significantly in Portugal. Additionally, the fixed-value thresholds can be directly compared to previous studies and agree with the current weather warning definition.

2.3 | ERA5 Reanalysis

To categorise the two selected case studies according to the synoptic-scale environment, the fifth generation of atmospheric reanalysis (ERA5) products, produced by the European Centre for Medium-range Weather Forecasts (ECMWF), were used. This reanalysis blends heterogeneous observational and numerical weather prediction (NWP) model information through data assimilation, where the model information is provided by a short forecast initiated from a previous cycle (Hacker et al. 2018; Hersbach et al. 2020). In ERA5, the assimilation system uses a 12-h window, in which observations are used from 0900 to 2100 UTC and from 2100 to 0900 UTC of the next day. ERA5 data is defined over a 0.25° latitude × 0.25° longitude grid, corresponding to a spatial resolution of 20–30 km. Data were retrieved from the Copernicus Climate Change Service (C3S, https://cds.climate.copernicus.eu/, accessed on 18 May 2023) (Hersbach et al. 2023a, 2023b) Climate Data Store platform, within the Euro-Atlantic geographical sector (30°–60° N, 30° W–10° E), with hourly resolution.

Although ERA5-land offers a finer spatial resolution than ERA5, ERA5-land only provides land surface fields such as precipitation, skin temperature, 2 m temperature and surface heat fluxes, among others (Muñoz-Sabater et al. 2021). Therefore, ERA5 was chosen to analyse the synoptic-scale circulation and thermodynamic conditions associated with heavy precipitation events.

The analysed variables comprise the mean sea level pressure (MSLP), 10 m zonal (u) and meridional (v) wind components, total column cloud ice water (TCCIW) and total column cloud liquid water (TCCLW). The geopotential height (Z) and air

temperature (T) on different isobaric levels (850, 500, 350 and 250 hPa) were analysed. Furthermore, the Convective Available Potential Energy (CAPE) (Bluestein and Jain 1985), convective inhibition (CIN) (Bluestein and Jain 1985), K-index (DeRubertis 2006) and TT (total–totals) index (Peppler and Lamb 1989) were also analysed (Table S4 and Figure S1). In addition to the variables mentioned, relative humidity and specific humidity at 850 hPa were also used for the calculation of equivalent potential temperature (θ_e), as described in Section 2.5.

2.4 | Definition of Indices

Different indices were used to assess the climatology of precipitation events in Portugal, adapted from Llasat et al. (2021). To calculate the indices presented in this section, hourly precipitation totals were obtained by summing 10-min amounts from each WS (AcP—hourly accumulated precipitation). After calculating the AcP, a second sum was made, this time for the respective season (winter—DJF, spring—MAM, summer—JJA, autumn—SON) for each of the 23 years (2000–2022). Finally, to calculate the average, the sum was divided by 23, generating the climatological seasonal average of accumulated precipitation, according to the following equations:

- Seasonal mean precipitation ($\overline{\text{TP}}_{\text{Season}}$): Climate-mean of total precipitation, in mm, observed in each season (winter, spring, summer and autumn):

$$\overline{\text{TP}}_{\text{Season}} = \frac{1}{n} \sum_{i=1}^{n} \text{AcP}_i \tag{1}$$

where, i = year, n = 23 and AcP is defined by:

$$\text{AcP} = \sum_{h=1}^{m} \text{TP} \tag{2}$$

h = hour, m = number of hours per station and TP represents hourly precipitation totals.

- Beta mean ($\overline{\beta}_{\text{Season}}$): Climate-mean ratio between total precipitation in a given season (DJF, MAM, JJA, SON) and total annual precipitation:

$$\overline{\beta}_{\text{Season}} = \frac{1}{n} \sum_{i=1}^{n} \frac{\text{TP}_{\text{Season}}}{\text{TP}_{\text{Annual}}} \tag{3}$$

This index was adapted for different thresholds of hourly precipitation intensity (I), namely for heavy precipitation events, that is, corresponding to yellow ($10 \leq I < 20\,\text{mm h}^{-1}$), or orange and red warnings, the latter two being grouped into a single index ($I \geq 20\,\text{mm h}^{-1}$):

$$\overline{\beta}_{\text{Season (Yellow)}} = \frac{1}{n} \sum_{i=1}^{n} \frac{\text{TP}_{\text{Season}}\left(10 \leq I < 20\,\text{mm h}^{-1}\right)}{\text{TP}_{\text{Season}}} \tag{4}$$

$$\overline{\beta}_{\text{Season (Orange and Red)}} = \frac{1}{n} \sum_{i=1}^{n} \frac{\text{TP}_{\text{Season}}\left(I \geq 20\,\text{mm h}^{-1}\right)}{\text{TP}_{\text{Season}}} \tag{5}$$

2.5 | Equivalent Potential Temperature

The wet-bulb potential temperature or equivalent potential temperature (θ_e), which are conserved for reversible moist adiabatic processes, are commonly used to diagnose frontal systems (Dacre et al. 2012; Pinto and Belo-Pereira 2020) and to diagnose tongues of warm and moist air. In this study, the equivalent potential temperature (θ_e) at 850 hPa was used, following the calculation method presented by Bolton (1980):

$$\begin{aligned} \theta_e = \quad & T_K \left(\frac{1000}{p} \right)^{0.2854\left(1 - 0.28 \times 10^{-3} r\right)} \\ & \times \exp\left[\left(\frac{3.376}{T_L} - 0.00254 \right) \times r \left(1 + 0.81 \times 10^{-3} r\right) \right] \end{aligned} \tag{6}$$

T_K, p and r are the absolute temperature (in K), pressure (in hPa) and mixing ratio (expressed in g kg^{-1}) at 850 hPa, respectively. In this study, the mixing ratio (r) was replaced by specific humidity ($r \approx q$), because the mixing ratio and specific humidity (q) tend to be very similar (Peixoto and Oort 1984; Dee and Da Silva 2003). T_L is the lifting condensation level temperature that can be obtained by (Bolton 1980):

$$T_L = \frac{1}{\frac{1}{T_K - 55} - \frac{\ln(\text{RH} / 100)}{2840}} + 55 \tag{7}$$

T_K and RH are absolute temperature (in K) and relative humidity (in %), respectively.

3 | Results

3.1 | Spatial–Temporal Characterisation of Seasonal Precipitation in Portugal

The characterisation of seasonal precipitation in Portugal is presented in Figure 2a–d, in which a large seasonal and spatial variability is observed, with a strong north–west to south–east gradient. The spatial variation was assessed through a spatial inverse distance weighting (IDW) of the recorded precipitation data from the surface WSs. This pattern can be largely explained by the greater exposure of the Atlantic-facing (windward side) mountain areas in the north to the maritime air masses from the North Atlantic, whereas inner areas are relatively sheltered from their direct influence (leeward side), besides the fact that higher latitudes are also more exposed to frontal systems. In effect, northward of the Tagus River, the east–west gradient is explained by the presence of the mountain ranges (Figure 1a) that promote condensation barrier effects (Trigo et al. 2008; Ramos, Trigo, and Liberato 2014; Santos and Belo-Pereira 2022). The observed gradient highlights the great influence of the orography on precipitation patterns and, consequently, on the Portuguese landscape and ecosystems.

Figure 2e–h depict a great seasonal variation in the β-index, with the winter months presenting the highest share of total annual precipitation (high β-index values), highly contrasting with the much drier summer and spring seasons (low β-index values). During winter (DJF), the greatest contribution to total annual precipitation is observed in the westernmost coastal
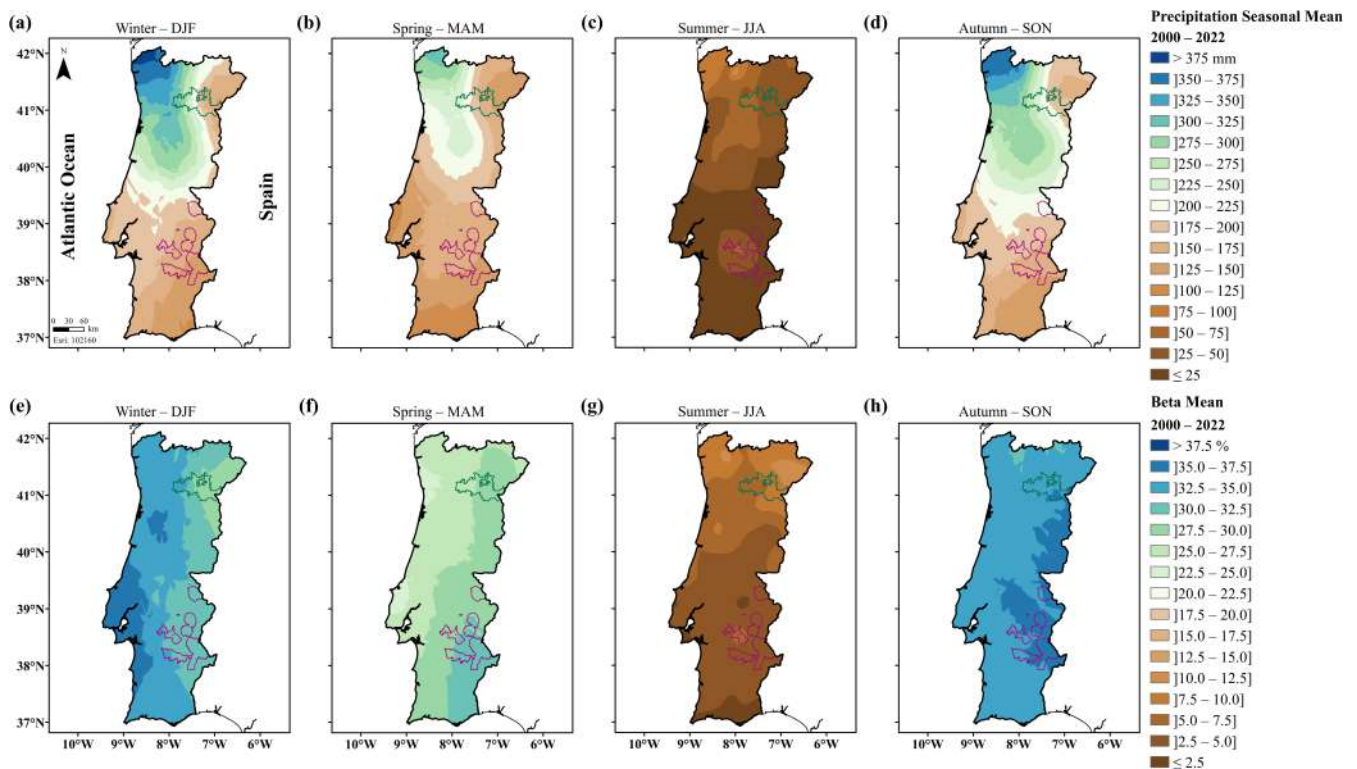
FIGURE 2 | (a–d) Spatial representation of the precipitation seasonal mean (in mm) and (e–h) seasonal beta mean index (in %) for (a, e) winter, (b, f) spring, (c, g) summer and (d, h) autumn, derived from the 63 surface weather stations (see locations in Figure 1b).

areas (Figure 2e), with a maximum in the centre/south region (> 35%), highlighting the key role played by the Atlantic low-pressure systems in the total precipitation. In spring (MAM), the spatial contribution to the total annual precipitation is more homogeneous throughout the country (Figure 2f), but with higher values occurring in the inner regions. These contributions range from 25% to 33%, particularly in Southern Portugal (Alentejo region), where values exceed 30%. In summer (JJA), a greater contribution is observed in the north–east region of Portugal (Figure 2g, Douro region), between 10.0% and 12.5%, with lower values in the centre and south regions (< 5.0%). The north–east of Portugal features complex orography, which is favourable to the generation of updrafts during relatively warm weather conditions, thus allowing the formation of cumulonimbus clouds (Ćurić et al. 2003). A consistently higher number of summertime lightning discharges in North–eastern Portugal was found (Santos et al. 2012; Sousa et al. 2013). Finally, during autumn (SON), the weather conditions in the inner regions are frequently influenced by the contrast between relatively cooler and moist air masses coming from the Atlantic Ocean and still warm Iberian continental air masses (Martín et al. 2004; Valero et al. 2009; Ramos et al. 2011), which promote instability and explain the highest values of the β-index (> 35%) over these areas (Figure 2h). These results are consistent with a recent study (Santos and Belo-Pereira 2022), which showed the existence of maximum occurrences of heavy precipitation associated with RemL (remote lows, centred near the British Isles or over the Bay of Biscay) events between October and November.

The contribution of mean seasonal precipitation taking into account the most severe precipitation thresholds, namely for YWs and ORWs, is presented in Figure 3. The identified patterns are identical to those described in Figure 2e–h, observing a greater contribution in the coastal region, with a maximum in the central/south region in winter, > 11% for YWs (Figure 3a) and from 1% to 2% for ORWs (Figure 3e). In spring (Figure 3b), a higher value of the β-index is observed in the south for YWs (> 7%), whereas it does not exceed 2% for ORWs in the central/south (Figure 3f). In summer, a greater contribution is observed in the north–east and central regions for YWs (Figure 3c), with a maximum of ~8% while being < 4% for the severest events (Figure 3g). As for winter, in autumn there is also a greater contribution of extreme events to total precipitation, mostly in the southern and centre regions, being > 11% for YWs (Figure 3d) and > 6% for ORWs (Figure 3h).

3.2 | Climatology of Heavy Precipitation Events

3.2.1 | Portugal

The interannual variation in the number of extreme precipitation events related to YWs ($10 \leq I < 20\,\mathrm{mm\,h^{-1}}$) and to ORWs ($I \geq 20\,\mathrm{mm\,h^{-1}}$) is presented in Figure 4a, illustrating a large interannual variability, with the number of YW events varying between 100 in 2012 and 285 in 2022. ORW events vary between 11 (in 2000, 2001, 2004, 2015 and 2017) and 43 events (in 2010). Typically, years with fewer extreme precipitation events, namely 2004, 2005, 2012 and 2017, are associated with years in which severe/extreme meteorological drought conditions occurred over most of the Portuguese territory (Drought Monitoring—IPMA 2024).
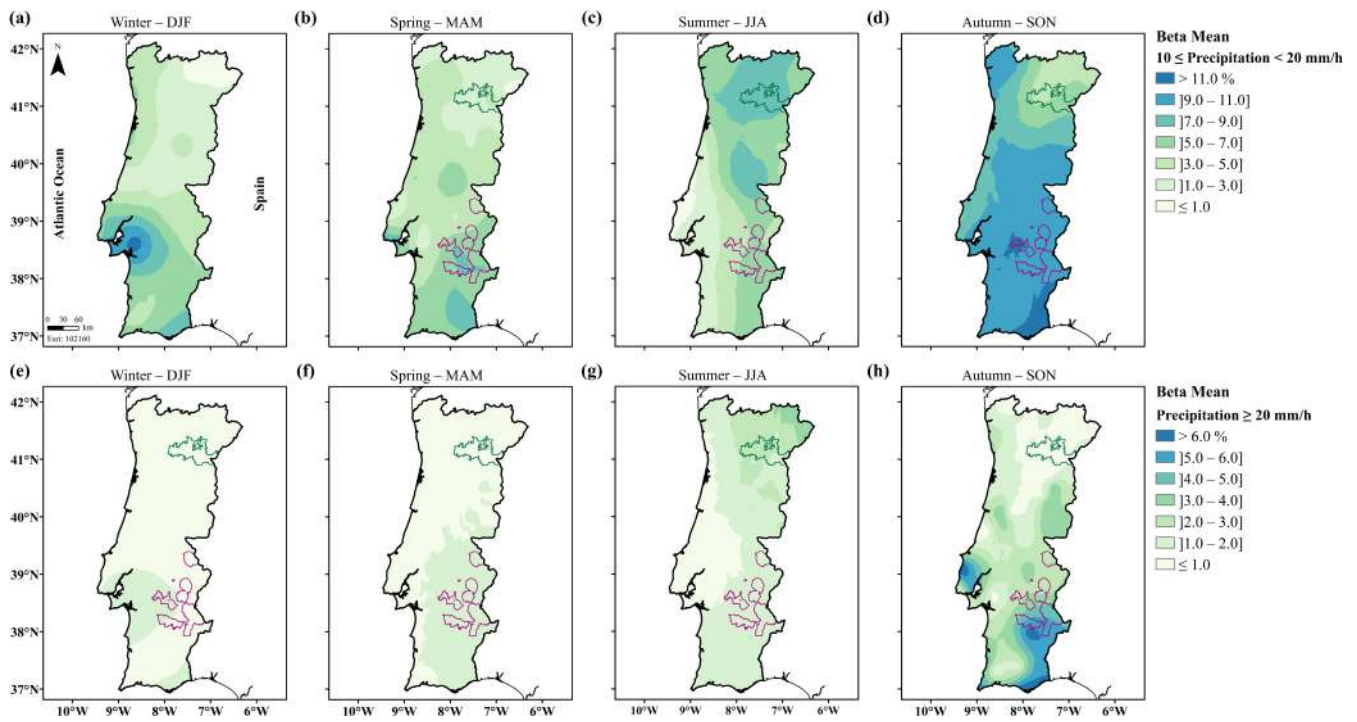
FIGURE 3 | Spatial representation of the seasonal beta mean index (in %) associated with hourly precipitation events for (a–d) $10 \leq I < 20 \, \text{mm h}^{-1}$ and (e–h) $I \geq 20 \, \text{mm h}^{-1}$ for (a, e) winter, (b, f) spring, (c, g) summer and (d, h) autumn, derived from the 63 surface weather stations (see locations in Figure 1b), where I is the hourly precipitation intensity.
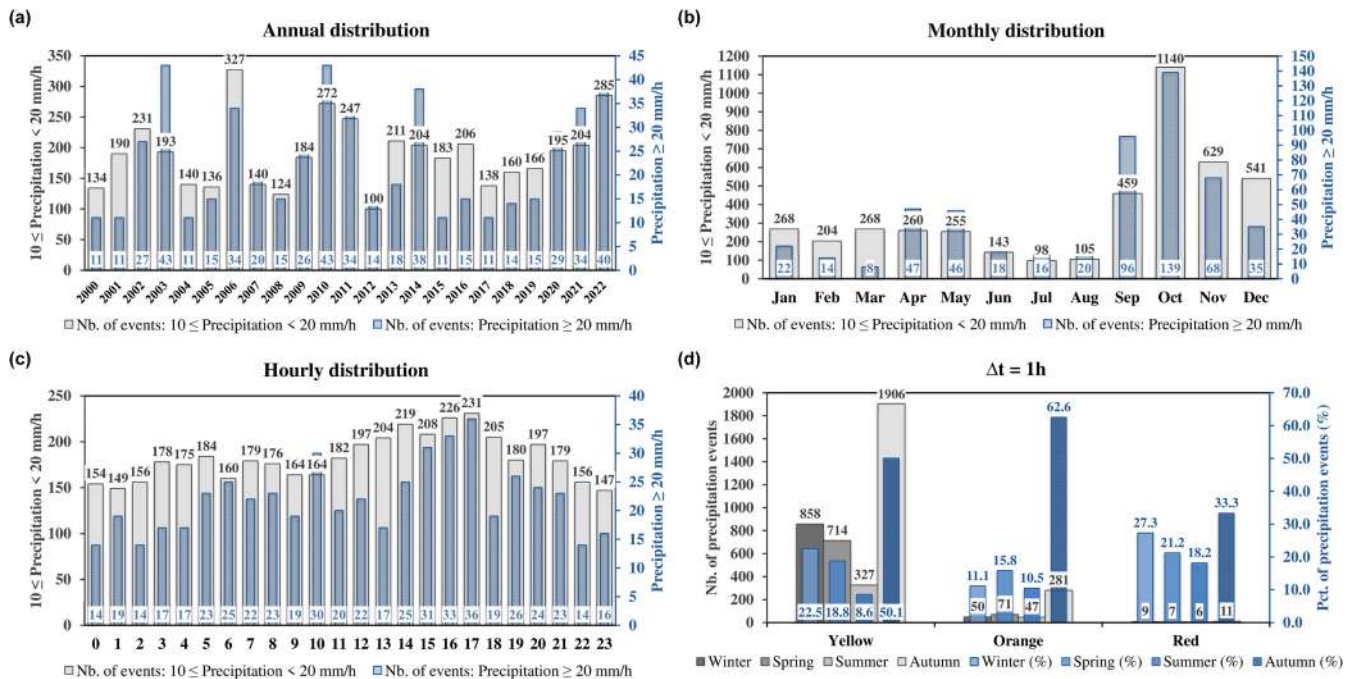
FIGURE 4 | Histogram of the (a) annual, (b) monthly and (c) hourly distribution of precipitation events identified for $10 \leq I < 20 \, \text{mm h}^{-1}$ (grey, left axis) and $I \geq 20 \, \text{mm h}^{-1}$ (blue, right axis), (d) the number of precipitation events identified (grey gradient, left axis) and total percentage (blue gradient, right axis), for yellow, orange and red IPMA warnings, for a time lag of $\Delta t = 1 \, \text{h}$, derived from the 63 surface weather stations (see locations in Figure 1b).

The seasonality in the number of extreme precipitation events in Portugal (Figure 4b) highlights a pronounced maximum between September and December for the (YW) events. For the ORW (ORW) events, one pronounced maximum is found in September–October and a secondary maximum in April–May. This is consistent with Santos and Belo-Pereira (2019), who showed the existence of two maxima for the episodes associated with regional lows (RegL), thus suggesting a closer relationship

of RegL events with convective systems. In summer, a lower number of occurrences of extreme events is shown, despite presenting a greater number of ORW events when compared to February–March. These occasional episodes are generally connected to strong local convective activity (Santos et al. 2012; Sousa et al. 2013; Santos and Belo-Pereira 2019). This can be confirmed by the spatial distribution of the mean number of precipitation events for a 10-year period (Figure S2).

The diurnal cycle (Figure 4c) for YW events hints at a late-afternoon maximum (17 UTC), decaying throughout the night. Furthermore, for ORW events, a noticeable maximum is clear in the afternoon. However, a slightly higher number of occurrences is also observed in the morning, with the maximum occurring at 10 UTC. The prominent late-afternoon peak is related to the enhancement of convective activity favoured by daytime heating and subsequent mature convective systems (Hoinka and Castro 2003; Kaltenböck et al. 2009; Burcea et al. 2016).

To better understand the event duration, we analysed the distribution of precipitation events applying specific time lags: $\Delta t = 1\,h$, $\Delta t = 3\,h$ and $\Delta t = 6\,h$, that is, precipitation events lagged by less or equal to 3 h ($\Delta t = 3\,h$) were treated as a single event and the same for 6 h intervals ($\Delta t = 6\,h$). This analysis helps identify how the frequency and intensity of precipitation events evolve when considering consecutive intervals, which is critical for assessing their persistence and impact over short-term periods. The distribution of the number of events for a time lag of $\Delta t = 1\,h$ (Figure 4d) associated with YW presents a pronounced maximum in autumn (1906), that is, ~50% of the total number of YW events, followed by winter with 22%. Further, for orange warnings ($20 \leq I < 40\,mm\,h^{-1}$), a higher percentage of occurrences is found in autumn (281), followed by spring (71 events, 16%). For

red warnings ($I \geq 40\,mm\,h^{-1}$), autumn also has a higher percentage of occurrences (11 events, 33%), followed by winter (9 events, 27%). The distribution of the number of precipitation events for the different thresholds and the respective percentage for a time lag of $\Delta t = 3\,h$ and $\Delta t = 6\,h$ is shown in Figure S3a,b. For yellow, orange and red warning events, the outcomes are very similar regardless of the time lag; noteworthy, a greater difference between $\Delta t = 1\,h$ and $\Delta t = 3\,h$ is observed. However, a steeper decrease in the number of events from yellow to orange and red warnings is observed, suggesting that events with higher precipitation amounts usually have a relatively short lifecycle. Moreover, events associated with orange and red warnings tend to contribute more to total daily precipitation (Figure S4). Red warning events have a greater contribution in summer and autumn, 86% and 58%, respectively, with their contribution being less significant in spring (47%). Orange warning events also hint at a higher contribution in summer (75%) and spring (61%), also showing the highest contributions to total daily precipitation in spring. YW events depict a smaller contribution to total daily precipitation, with the highest contribution in summer (60%).

3.2.2 | Douro Region

A more detailed characterisation of the Douro region is now presented (Figure 5). This region is characterised by smooth annual variability (Figure 5a), with 2003 and 2021 presenting 10 YW events, followed by 2000, 2002 and 2010, with nine events. In turn, the largest number of ORW events occurred in 2006 and 2018, with three events each. The seasonal cycle for YW (Figure 5b) presents one pronounced maximum between September and December and a secondary peak between April and June, this second maximum overlapping with the ORW
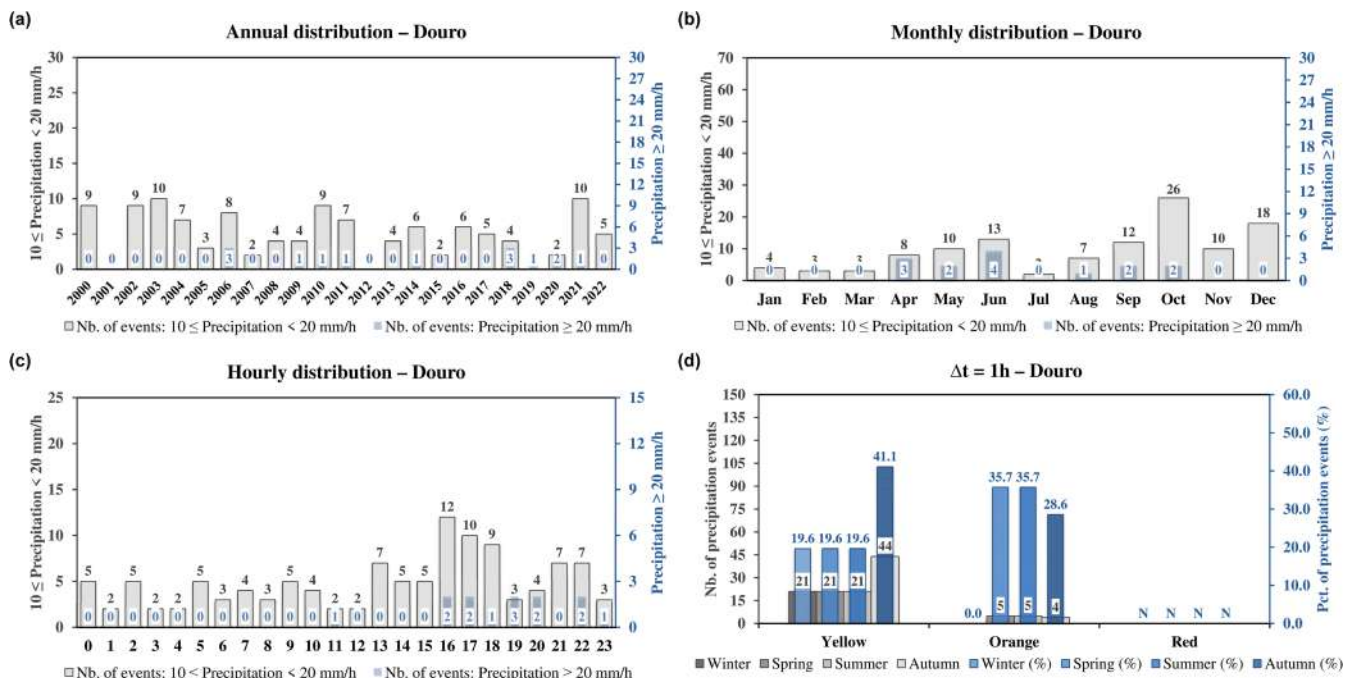
FIGURE 5 | Histogram of the (a) annual, (b) monthly and (c) hourly distribution of precipitation events identified for $10 \leq I < 20\,mm\,h^{-1}$ (grey, left axis) and $I \geq 20\,mm\,h^{-1}$ (blue, right axis), (d) the number of precipitation events identified (grey gradient, left axis) and total percentage (blue gradient, right axis) for yellow, orange and red IPMA warnings, for a time lag of $\Delta t = 1\,h$, for the three surface weather stations that characterise the Douro region.

maximum. The diurnal cycle (Figure 5c) presents a greater number of occurrences for mid-afternoon (16 UTC), which is verified in the two thresholds. At last, the number of precipitation events (Figure 5d) associated with YW peaks in autumn with 44 events, corresponding to 41%, with the remaining seasons presenting 21 events each. For orange-warning ($20 \leq I < 40\,mm\,h^{-1}$) events, 5 events in both spring and summer are found, 4 in autumn and no events in winter. No red-warning events were identified. Concerning the time lags of $\Delta t = 3\,h$ and $\Delta t = 6\,h$, for the Douro region, the results were similar to those found for the whole country, despite the necessarily lower number of occurrences (Figure S3c,d).

3.2.3 | Alentejo Region

According to the climatology for Alentejo (Figure 6), this region is characterised by high annual variability (Figure 6a). The highest number of YW events (40) occurred in 2006, followed by 2008 (29). As for ORW, the maximum number of events was recorded in 2003 (27), followed by 2020 (6). The seasonal cycle (Figure 6b) presents one pronounced maximum in October for the YW events (100). For ORW, two maxima are observed, the first in April, with 27 events and the second in October, with 18 events. The diurnal cycle (Figure 6c) related to YW events displays two maxima in the afternoon, the first between 13 and 15 UTC and the second between 17 and 18 UTC. For ORW, three maxima are apparent, the first in the late morning, followed by two others in the afternoon, at 15–16 UTC and 19–20 UTC. The distribution of the YW events for the 1-h time lag (Figure 6d) reveals a pronounced maximum in autumn (144), that is, approximately 46% of events, followed by spring with 24%. Moreover, for orange warnings, autumn presents a higher percentage of occurrences (23 events, 54%), followed by spring (14 events, 32.6%). For red warnings, spring also reveals a higher percentage of occurrences (43%), followed by winter (29%). The distribution of the number of precipitation events for the different thresholds and the respective percentage for 3- and 6-h time lags (Figure S3e,f) reveals a more marked decrease for YW events, remaining nearly constant for ORW.

3.3 | Case Studies

3.3.1 | Douro Region

This section examines in detail the synoptic environment associated with a heavy rainfall event in the Douro region. The selected event occurred on the afternoon of 28 May 2018, in which precipitation values of around 90 mm were recorded in less than 2 h, also accompanied by heavy hailfall, inflicting serious damage to vineyards and grapevines—evidence reported by the winemaking company (https://porttoportwine.blogspot.com/2018/, accessed on 3 January 2025).

A cold core cyclone at 500 hPa, centred over Western Iberia, is visible in Figure 7. At the surface, a low-pressure system is located south–east of the mid-level low, revealing a baroclinic structure (Figure 7a). The existence of this cold air mass aloft in North–western Iberia (Figure 7b), coupled with an increase in near-surface temperatures, ranging from 18°C to 25°C during the afternoon (not shown), enables the establishment of an important lapse rate, indicating thermodynamic instability, as will be evidenced by the instability indices. At 850 hPa, the low-level cyclonic circulation centred on IP (Figure 7b), extending to the western region of the Bay of Biscay, drives north–westerly winds
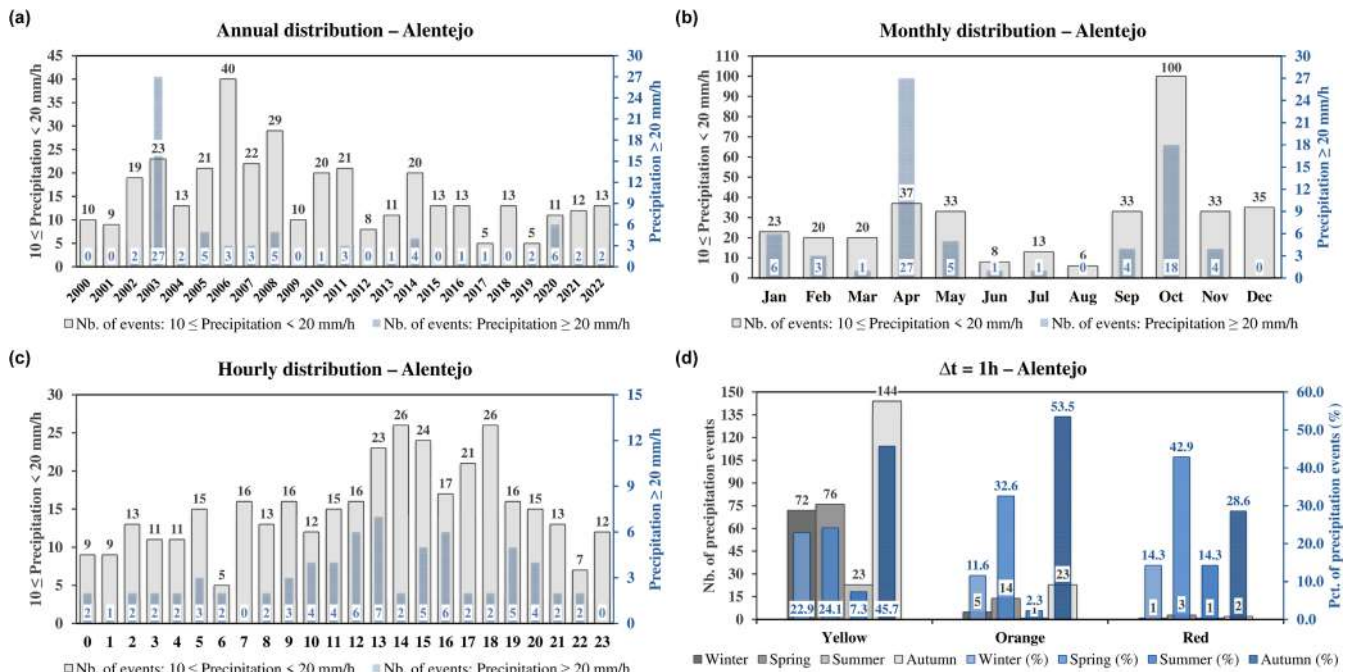
FIGURE 6 | Histogram of the (a) annual, (b) monthly and (c) hourly distribution of precipitation events identified for $10 \leq I < 20\,mm\,h^{-1}$ (grey, left axis) and $I \geq 20\,mm\,h^{-1}$ (blue, right axis), (d) number of precipitation events identified (grey gradient, left axis) and total percentage (blue gradient, right axis) for yellow, orange and red IPMA warnings, for a time lag of $\Delta t = 1\,h$, for the four surface weather stations that characterise the Alentejo region.
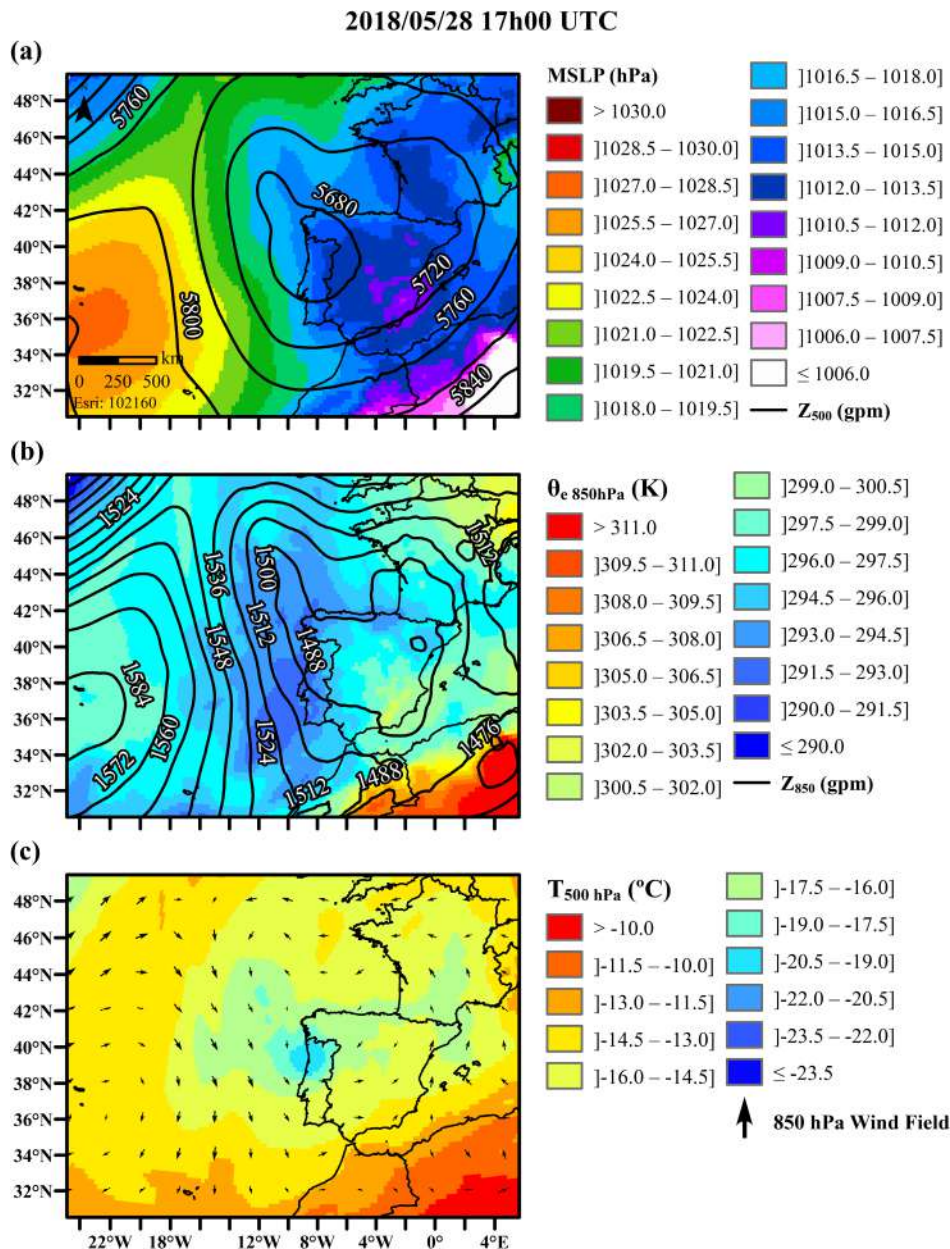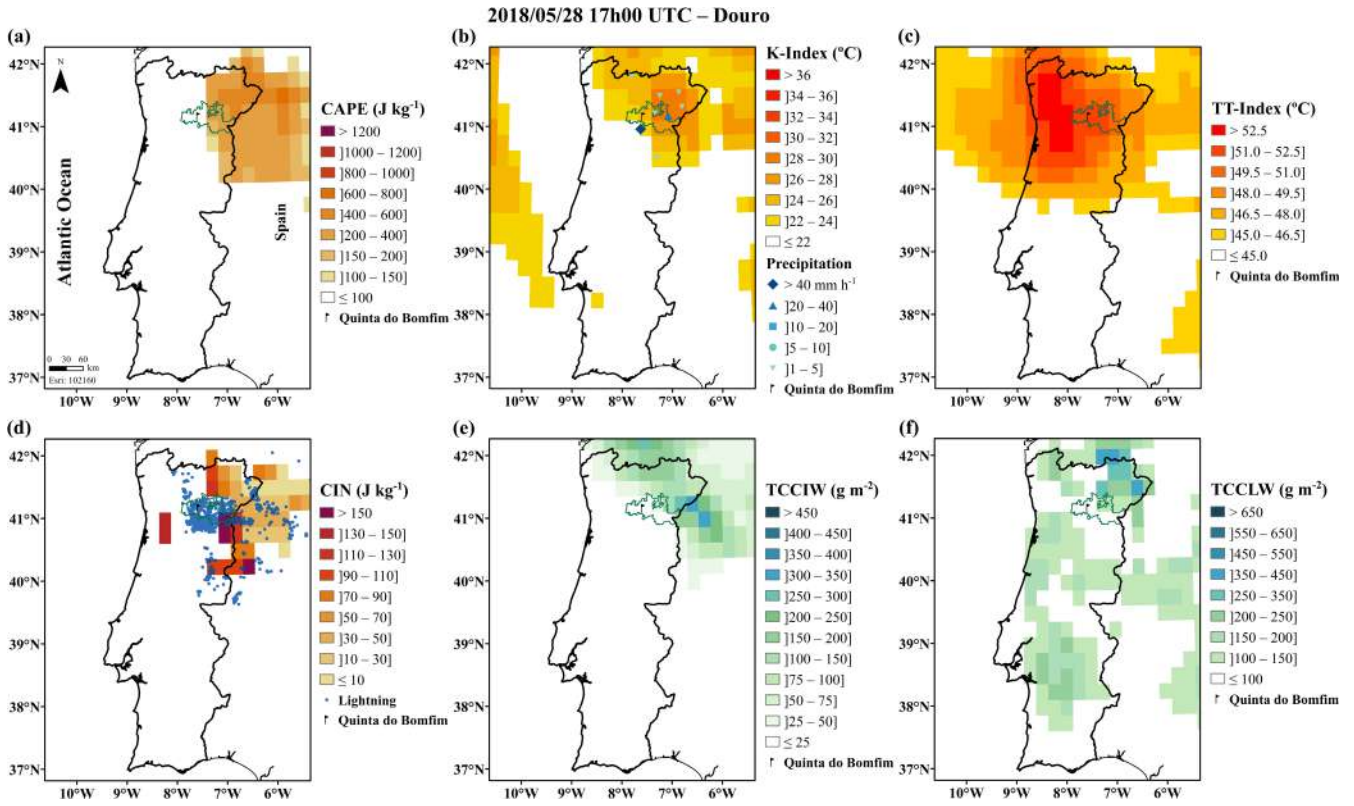
FIGURE 7 | ERA5 reanalysis valid at 17 UTC on 28 May 2018, (a) mean sea-level pressure (MSLP) (in hPa, shading colours), and 500 hPa geopotential height (Z_{500}) (in gpm, contour lines represented in black, with a spacing of 40 gpm), (b) 500 hPa temperature (in °C, shading colours), and 850 hPa geopotential height (Z_{850}) (in gpm, contour lines represented in black, with a spacing of 12 gpm), (c) 850 hPa equivalent potential temperature ($\theta_{e\,850\,hPa}$) (in K, shading colours) and 850 hPa wind (vectors represented in black arrows).

towards the north–west of IP, causing an injection of moist air from the Atlantic coastal area of IP (Figure 7c). In Northern Portugal, contributing to reinforcing the east–west contrast between the air masses, depicted by the zonal gradient of θ_e (Figure 7c). This low-pressure system is the result of the evolution of a cut-off low located north–east of the Azores archipelago on 21 May (Figures S5a, S6a and S7a), which intensified as it moved south–east towards the Madeira Island and then moved north–east towards the IP, as demonstrated by the geopotential and temperature fields at 250, 350 and 500 hPa (Figures S5–S7).

The presence of atmospheric instability is diagnosed by the thermodynamic indices presented in Figure 8a–c, respectively. All these indices reveal higher instability in Northern Portugal.

Nevertheless, the TT-index shows a larger area of instability, with maximum values in the north–west of Portugal, whereas CAPE and K-index display smaller areas, with greater values in the north–east region extending to Spain. The spatial distribution of the atmospheric lightning discharges, which affected the Douro vineyards, shows a greater agreement with the pattern of the K-index when compared to the other indices. The CIN index shows values of around 50–150 J kg^{-1} in North–eastern Portugal near the Spanish border, in areas where thunderstorms occurred, as shown by the lightning observations (Figure 8d). Given the complexity of the terrain in this area, it is not surprising that the orographic forcing may have been sufficient to overcome the CIN, thereby allowing convective cells to develop and mature.

FIGURE 8 | ERA5 reanalysis valid at 17 UTC on 28 May 2018, (a) convective available potential energy (CAPE) (in J kg^{-1}, shading colours), (b) K-index (in °C, shading colours) and maximum precipitation observed in the hour before and after 17 UTC measured in the surface weather stations, (c) total-totals index (TT-index) (in °C, shading colours), (d) convective inhibition (CIN) (in J kg^{-1}, shading colours) and lightning in the hour before and after 17 UTC (points represented in blue), (e) total column cloud ice water (TCCIW) (in g m^{-2}, shading colours) and (f) total column cloud liquid water (TCCLW) (in g m^{-2}, shading colours).

In the area where the thunderstorms occurred, one station recorded a precipitation intensity of 45 mm h^{-1} and another of 21 mm h^{-1}. The other stations in the vicinity recorded values between 1 and 5 mm h^{-1}. Given the relatively small scale of the convective cells, it is very likely that the representativeness of the network of surface WSs may be insufficient to accurately capture the spatial distribution of the precipitation amounts that effectively occurred.

The amount of ice and liquid water in clouds is shown in Figure 8e,f, respectively. A greater concentration of ice and liquid water is observed in the northern inner region, despite a high dispersion of liquid water across land areas. Despite a slight spatial lag, the combination of the K-index with the presence of cloud ice water is useful for diagnosing the presence of deep convection, which is in accordance with Cruz et al. (2023).

3.3.2 | Alentejo Region

For the Alentejo region, the selected event occurred in the early hours of 14 September 2021, in which hourly precipitation values greater than 35 mm were recorded at the 'S. Pedro do Corval' station (EMA 840). Figures 9 and 10 show the evolution of the synoptic conditions for the 3 days before the event date. On 11 September at 00 UTC, a frontal system is visible north–eastwards of the Azores (Figures 9a and 10a). At this

stage, the mid-level low is located to the south–west of the low-pressure centre at the surface, thus favouring the development of the system (Figure 9a). The warm sector is characterised by θ_e varying between 298 K and 302 K (Figure 10a). Over the next 36 h, the surface low deepens as the occlusion process continues, with the warm sector becoming smaller and the mid-level low progressively aligned with the surface low-pressure centre. On 13 September at 00 UTC, the low-pressure centre at the surface reached its maximum strength, with a minimum MSLP < 1006 hPa (Figure 9e), forming a cold core cyclone, with a minimum θ_e in its centre (Figure 10e), visible also at 500 hPa (not shown). In the next 36 h, the low-pressure system weakens as it approaches the IP (Figure 9e–h), favouring the advection of relatively warm and moist air masses from the subtropical North Atlantic towards Western Iberia (Figure 10e–h).

These synoptic conditions fostered atmospheric instability and the occurrence of thunderstorms in mainland Portugal (Figure 11a–d). The atmospheric discharges are mostly concentrated in the south (Figure 11d), where hourly precipitation in some stations exceeds 20 mm h^{-1}. This area also presents strong instability, illustrated by CAPE values > 800 J kg^{-1} (Figure 11a) and high values of cloud ice and liquid water contents (Figure 11e–f). Isolated thunderstorms have also developed over the sea and in Spain, in regions with low CIN values (< 50 J kg^{-1}). In Spain, the area of thunderstorms corresponds to the areas with the highest TCCIW and TCCLW values.
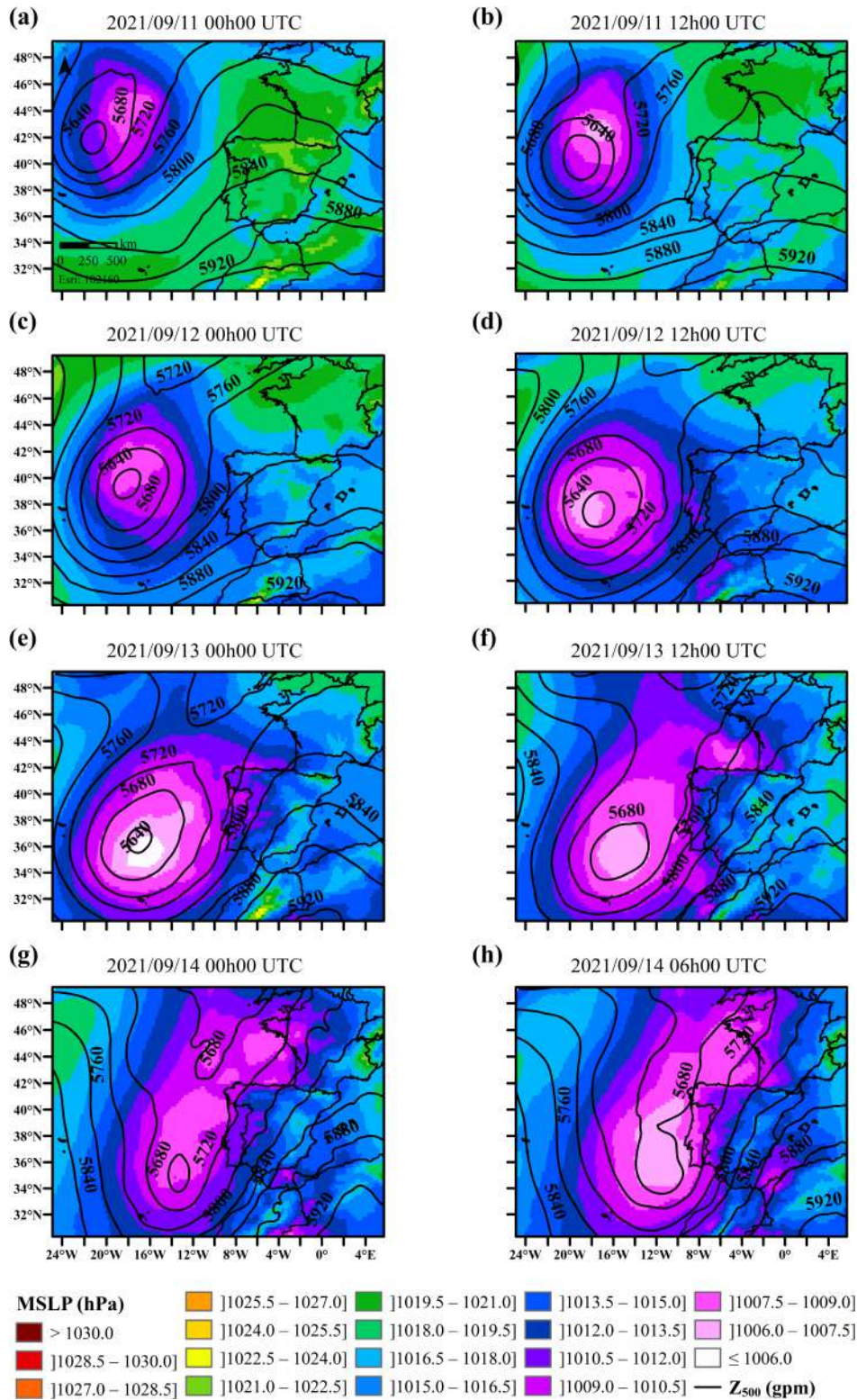
FIGURE 9 | (a–h) Mean sea-level pressure (MSLP) (in hPa, shading colours), and 500 hPa geopotential height (Z_{500}) (contour lines represented in black, with a spacing of 40 gpm). ERA5 reanalysis data from 00 UTC on 11 September 2021 to 06 UTC on 14 September 2021.

4 | Discussion and Conclusions

This study provides the first comprehensive analysis of extreme precipitation events in Portugal, based on hourly observations. This analysis covers the period from 2000 to 2022 (23 years)

and uses 10-min precipitation observations from a network of 71 surface WSs. In addition to the climatological characteristics of extreme precipitation events (spatial and temporal variability, including seasonality and daily cycle), an analysis is also presented of their connections to the synoptic scale drivers,
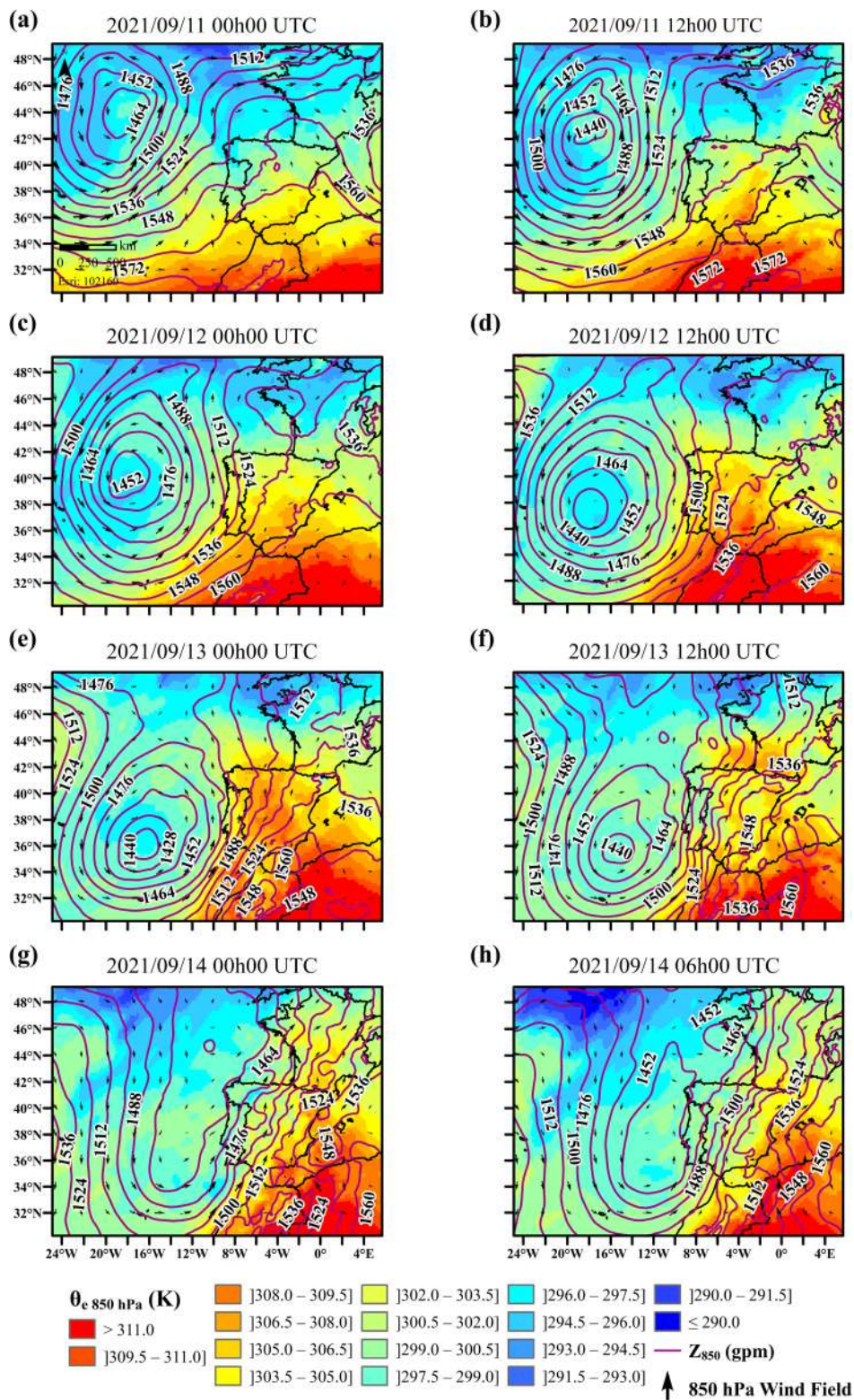
FIGURE 10 | (a–h) 850 hPa equivalent potential temperature ($\theta_{e\ 850\ hPa}$) (in K, shading colours), 850 hPa geopotential height (Z_{850}) (contour lines represented in magenta, with a spacing of 12 gpm) and 850 hPa wind (vectors represented in black arrows). ERA5 reanalysis data from 00 UTC on 11 September 2021 to 06 UTC on 14 September 2021.

through two case studies for two main wine-growing regions in Portugal.

The spatial distribution of precipitation reveals a high variability, with a south–east to north–west gradient, the

north–westernmost region showing the highest precipitation amounts. The β-index, considering the most severe precipitation thresholds, also presents a large spatial variability, with winter showing a greater contribution to total precipitation, associated with frequent travelling lows that cross the
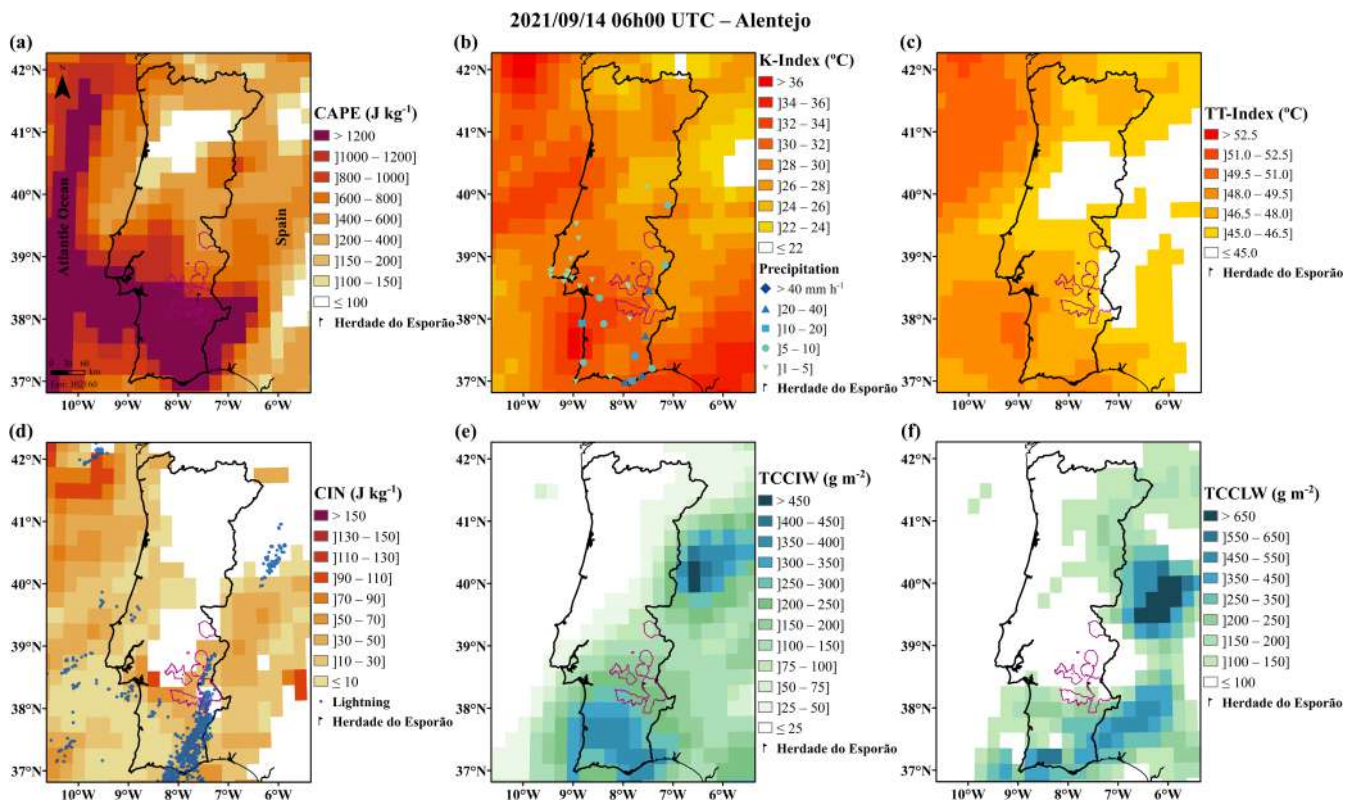
FIGURE 11 | ERA5 reanalysis valid on 06 UTC on 14 September 2021 (a) convective available potential energy (CAPE) (in J kg^{-1}, shading colours), (b) *K*-index (in °C, shading colours) and maximum precipitation observed in the hour before and after 17 UTC measured in the surface weather stations, (c) total-totals index (TT-index) (in °C, shading colours), (d) convective inhibition (CIN) (in J kg^{-1}, shading colours) and lightning in the hour before and after 17 UTC (points represented in blue), (e) total column cloud ice water (TCCIW) (in g m^{-2}, shading colours) and (f) total column cloud liquid water (TCCLW) (in g m^{-2}, shading colours).

Atlantic, when compared to autumn, and particularly, to summer and spring.

The seasonality of the extreme precipitation events in mainland Portugal presents a pronounced maximum between September and December and a secondary peak in April/May, this latter being more pronounced in the southern inner region (Alentejo) when compared with the northern inner region (Douro). These results are consistent with the study by Santos and Belo-Pereira (2019), which showed the existence of two marked maxima in spring and autumn associated with RegL events and a maximum in autumn for remote low events. Further, the diurnal cycle hints at a maximum in the afternoon, coherent with the highest frequency of thunderstorms during the afternoon (Santos et al. 2012; Sousa et al. 2013; Santos and Belo-Pereira 2019). Extreme precipitation events tend to make a greater contribution to total daily precipitation, mostly in spring and summer. The complex orography and the contrast between colder and moister air masses, coming from the Atlantic Ocean, with the typically warm and dry continental air masses reinforce convection in summer and autumn (Ćurić et al. 2003; Martín et al. 2004; Valero et al. 2009; Ramos et al. 2011).

The events of 28 May 2018 and 14 September 2021 were selected in close collaboration with two winemaking companies, one based in the Douro region (Quinta do Bomfim) and the other in the Alentejo region (Herdade do Esporão). These events are selected because of their reported severity. In the first case, the

event of 28 May 2018 in the Douro region was associated with a cut-off low. The presence of a 500 hPa cold core centred over the surface low favours the presence of thermodynamic instability, which was identified by the stability indices derived from the ERA5 data. The *K*-index showed greater agreement with the spatial distribution of the observed lightning, suggesting greater skill in identifying favourable conditions to deep convection. The CIN showed values exceeding 100 J kg^{-1} in the vicinity of the areas where thunderstorms occurred, indicating that the orographic forcing may have been sufficient to overcome CIN, allowing convective cells to develop.

In the second case, the event of 14 September 2021 in the Alentejo region, the ERA5 reanalysis data revealed that this event was associated with a frontal system that developed north–east of the Azores and reached mainland Portugal in the final phase of its life cycle. In this case, thermodynamic indices based on ERA5 showed a clear agreement between the areas of greatest instability and the lightning spatial distribution.

These outcomes provide valuable information not only for future research but also for several socioeconomic sectors in the country, such as viticulture, for which the occurrence of extreme precipitation events (heavy rainfall and hailfall) represents a major natural hazard, often resulting in significant damage and losses. The analysis of the temporal distribution of the number of extreme precipitation events, particularly on a regional basis, is crucial to support decision-making in agricultural planning

and other socioeconomic sectors. Furthermore, the analysis and identification of the β-index for different seasons and the various precipitation thresholds were defined according to the warning criteria set by the Portuguese Weather Service.

Conflicts of Interest

The authors declare no conflicts of interest.

Data Availability Statement

ERA5 reanalysis data are available from the Climate Data Store database (https://cds.climate.copernicus.eu/). The weather station data can be requested by completing the form on the official website of the Portuguese Weather Service (IPMA—https://www.ipma.pt/en/siteinfo/contactar.jsp) or by emailing comercial@ipma.pt.

References

Alexandersson, H. 1986. "A Homogeneity Test Applied to Precipitation Data." *Journal of Climatology* 6, no. 6: 661–675.

Austin, M. E., and K. Bondari. 1988. "A Study of Cultural and Environmental Factors on the Yield of *Vitis Rotundifolia*." *Scientia Horticulturae* 34, no. 3–4: 219–227.

Belo-Pereira, M., E. Dutra, and P. Viterbo. 2011. "Evaluation of Global Precipitation Data Sets Over the Iberian Peninsula." *Journal of Geophysical Research: Atmospheres* 116, no. D20: 2010JD015481. https://doi.org/10.1029/2010JD015481.

Bluestein, H. B., and M. H. Jain. 1985. "Formation of Mesoscale Lines of Pirecipitation: Severe Squall Lines in Oklahoma During the Spring." *Journal of the Atmospheric Sciences* 42, no. 16: 1711–1732.

Bolton, D. 1980. "The Computation of Equivalent Potential Temperature." *Monthly Weather Review* 108, no. 7: 1046–1053. https://doi.org/10.1175/1520-0493(1980)108<1046:TCOEPT>2.0.CO;2.

Brunetti, M., M. Colacino, M. Maugeri, and T. Nanni. 2001. "Trends in Daily Intensity of Precipitation in Italy From 1951 to 1996." *International Journal of Climatology* 21, no. 3: 299–316. https://doi.org/10.1002/joc.613.

Buishand, T. A. 1982. "Some Methods for Testing the Homogeneity of Rainfall Records." *Journal of Hydrology* 58, no. 1–2: 11–27.

Burcea, S., R. Cică, and R. Bojariu. 2016. "Hail Climatology and Trends in Romania: 1961–2014." *Monthly Weather Review* 144, no. 11: 4289–4299. https://doi.org/10.1175/MWR-D-16-0126.1.

Cardoso, R. M., P. M. M. Soares, D. C. A. Lima, and P. M. A. Miranda. 2019. "Mean and Extreme Temperatures in a Warming Climate: EURO CORDEX and WRF Regional Climate High-Resolution Projections for Portugal." *Climate Dynamics* 52, no. 1–2: 129–157. https://doi.org/10.1007/s00382-018-4124-4.

Cardoso, R. M., P. M. M. Soares, P. M. A. Miranda, and M. Belo-Pereira. 2013. "WRF High Resolution Simulation of Iberian Mean and Extreme Precipitation Climate." *International Journal of Climatology* 33, no. 11: 2591–2608. https://doi.org/10.1002/joc.3616.

Casado, M. J., M. A. Pastor, and F. J. Doblas-Reyes. 2010. "Links Between Circulation Types and Precipitation Over Spain." *Physics and Chemistry of the Earth, Parts A/B/C* 35, no. 9–12: 437–447.

Cohuet, J. B., R. Romero, V. Homar, V. Ducrocq, and C. Ramis. 2011. "Initiation of a Severe Thunderstorm Over the Mediterranean Sea." *Atmospheric Research* 100, no. 4: 603–620. https://doi.org/10.1016/j.atmosres.2010.11.002.

Cortès, M., M. Turco, M. Llasat-Botija, and M. C. Llasat. 2018. "The Relationship Between Precipitation and Insurance Data for Floods in a Mediterranean Region (Northeast Spain)." *Natural Hazards and Earth System Sciences* 18, no. 3: 857–868. https://doi.org/10.5194/nhess-18-857-2018.

Costa, A. C., and A. Soares. 2008. "geoENV VI—Geostatistics for Environmental Applications. geoENV VI—Geostatistics for Environmental Applications." https://doi.org/10.1007/978-1-4020-6448-7.

Cruz, J., M. Belo-Pereira, A. Fonseca, and J. A. Santos. 2023. "Dynamic and Thermodynamic Drivers of Severe Sub-Hourly Precipitation Events in Mainland Portugal." *Atmosphere* 14, no. 9: 1–20. https://doi.org/10.3390/atmos14091443.

Ćurić, M., D. Janc, D. Vujović, and V. Vučković. 2003. "The Effects of a River Valley on an Isolated Cumulonimbus Cloud Development." *Atmospheric Research* 66, no. 1–2: 123–139. https://doi.org/10.1016/S0169-8095(02)00144-8.

Dacre, H. F., M. K. Hawcroft, M. A. Stringer, and K. I. Hodges. 2012. "An Extratropical Cyclone Atlas: A Tool for Illustrating Cyclone Structure and Evolution Characteristics." *Bulletin of the American Meteorological Society* 93, no. 10: 1497–1502. https://doi.org/10.1175/BAMS-D-11-00164.1.

Dee, D. P., and A. M. Da Silva. 2003. "The Choice of Variable for Atmospheric Moisture Analysis." *Monthly Weather Review* 131, no. 1: 155–171. https://doi.org/10.1175/1520-0493(2003)131<0155:TCOVFA>2.0.CO;2.

DeRubertis, D. 2006. "Recent Trends in Four Common Stability Indices Derived From US Radiosonde Observations." *Journal of Climate* 19, no. 3: 309–323. https://doi.org/10.1175/JCLI3626.1.

Drought Monitoring—IPMA. 2024. "Instituto Português do Mar e da Atmosfera." https://www.ipma.pt/pt/oclima/observatorio.secas/pdsi/apresentacao/evolu.historica/.

Esteban-Parra, M. J., F. S. Rodrigo, and Y. Castro-Diez. 1998. "Spatial and Temporal Patterns of Precipitation in Spain for the Period 1880–1992." *International Journal of Climatology* 18, no. 14: 1557–1574. https://doi.org/10.1002/(SICI)1097-0088(19981130)18:14<1557::AID-JOC328>3.0.CO;2-J.

Fonseca, A., H. Fraga, and J. A. Santos. 2023. "Exposure of Portuguese Viticulture to Weather Extremes Under Climate Change." *Climate Services* 30: 100357. https://doi.org/10.1016/j.cliser.2023.100357.

Fraga, H., A. C. Malheiro, J. Moutinho-Pereira, and J. A. Santos. 2012. "An Overview of Climate Change Impacts on European Viticulture." *Food and Energy Security* 1, no. 2: 94–110.

Frame, D., S. Rosier, I. Noy, et al. 2020. "Climate Change Attribution and the Economic Costs of Extreme Weather Events: A Study on Damages From Extreme Rainfall and Drought." *Climatic Change* 162, no. 2: 781–797. https://doi.org/10.1007/s10584-020-02729-y.

Hacker, J., C. Draper, and L. Madaus. 2018. "Challenges and Opportunities for Data Assimilation in Mountainous Environments." *Atmosphere* 9, no. 4: 127.

Hardie, W. J., and S. R. Martin. 2000. "Shoot Growth on De-Fruited Grapevines: A Physiological Indicator for Irrigation Scheduling." *Australian Journal of Grape and Wine Research* 6, no. 1: 52–58.

Hawcroft, M. K., L. C. Shaffrey, K. I. Hodges, and H. F. Dacre. 2012. "How Much Northern Hemisphere Precipitation Is Associated With Extratropical Cyclones?" *Geophysical Research Letters* 39, no. 24: 1–7. https://doi.org/10.1029/2012GL053866.

Hersbach, H., B. Bell, P. Berrisford, et al. 2023a. "ERA5 Hourly Data on Single Levels From 1940 to Present." https://cds.climate.copernicus.eu/cdsapp#!/dataset, https://doi.org/10.24381/cds.adbb2d47.

Hersbach, H., B. Bell, P. Berrisford, et al. 2023b. "ERA5 Hourly Data on Pressure Levels From 1940 to present." https://cds.climate.copernicus.eu/cdsapp#!/dataset, https://doi.org/10.24381/cds.bd0915c6.

Hersbach, H., B. Bell, P. Berrisford, et al. 2020. "The ERA5 Global Reanalysis." *Quarterly Journal of the Royal Meteorological Society* 146, no. 730: 1999–2049.

Hoinka, K. P., and M. D. E. Castro. 2003. "The Iberian Peninsula Thermal Low." *Quarterly Journal of the Royal Meteorological Society: A Journal of the Atmospheric Sciences, Applied Meteorology and Physical Oceanography* 129, no. 590: 1491–1511.

IPMA. 2024. "IPMA–Índice." https://www.ipma.pt/en/enciclopedia/otempo/sam/index.html?page=criterios.xml.

Jones, P. D., E. B. Horton, C. K. Folland, M. Hulme, D. E. Parker, and T. A. Basnett. 1999. "The Use of Indices to Identify Changes in Climatic Extremes." *Climatic Change* 42: 131–149.

Kaltenböck, R., G. Diendorfer, and N. Dotzek. 2009. "Evaluation of Thunderstorm Indices From ECMWF Analyses, Lightning Data and Severe Storm Reports." *Atmospheric Research* 93, no. 1–3: 381–396. https://doi.org/10.1016/j.atmosres.2008.11.005.

Karl, T. R., N. Nicholls, and A. Ghazi. 1999. "CLIVAR/GCOS/WMO Workshop on Indices and Indicators for Climate Extremes Workshop Summary BT–Weather and Climate Extremes: Changes, Variations and a Perspective From the Insurance Industry." *Weather and Climate Extremes*. 3–7.

Kostopoulou, E., and P. D. Jones. 2005. "Assessment of Climate Extremes in the Eastern Mediterranean." *Meteorology and Atmospheric Physics* 89, no. 1–4: 69–85. https://doi.org/10.1007/s00703-005-0122-2.

Lee, H., K. Calvin, D. Dasgupta, et al. 2023. "IPCC, 2023: Climate Change 2023: Synthesis Report, Summary for Policymakers." In *Contribution of Working Groups I, II and III to the Sixth Assessment Report of the Intergovernmental Panel on Climate Change*, edited by Core Writing Team, H. Lee, and J. Romero. Intergovernmental Panel on Climate Change (IPCC).

Liberato, M. L. R. 2014. "The 19 January 2013 Windstorm Over the North Atlantic: Large-Scale Dynamics and Impacts on Iberia." *Weather and Climate Extremes* 5, no. 1: 16–28. https://doi.org/10.1016/j.wace.2014.06.002.

Liberato, M. L. R., and R. M. Trigo. 2014. "Extreme Precipitation Events and Related Impacts in Western Iberia." *IAHS-AISH Proceedings and Reports* 363: 171–176.

Llasat, M. C., A. del Moral, M. Cortès, and T. Rigo. 2021. "Convective Precipitation Trends in the Spanish Mediterranean Region." *Atmospheric Research* 257: 105581. https://doi.org/10.1016/j.atmosres.2021.105581.

Martín, M. L., M. Y. Luna, A. Morata, and F. Valero. 2004. "North Atlantic Teleconnection Patterns of Low-Frequency Variability and Their Links With Springtime Precipitation in the Western Mediterranean." *International Journal of Climatology: A Journal of the Royal Meteorological Society* 24, no. 2: 213–230. https://doi.org/10.1002/joc.993.

Mills, G. F. 1995. "Principal Component Analysis of Precipitation and Rainfall Regionalization in Spain." *Theoretical and Applied Climatology* 50, no. 3–4: 169–183. https://doi.org/10.1007/BF00866115.

Moberg, A., and P. D. Jones. 2005. "Trends in Indices for Extremes in Daily Temperature and Precipitation in Central and Western Europe, 1901–99." *International Journal of Climatology* 25, no. 9: 1149–1171. https://doi.org/10.1002/joc.1163.

Moreno, M., L. Lombardo, A. Crespi, et al. 2024. "Space-Time Data-Driven Modeling of Precipitation-Induced Shallow Landslides in South Tyrol, Italy." *Science of the Total Environment* 912: 169166. https://doi.org/10.1016/j.scitotenv.2023.169166.

Muñoz-Sabater, J., E. Dutra, A. Agustí-Panareda, et al. 2021. "ERA5-Land: A State-Of-The-Art Global Reanalysis Dataset for Land Applications." *Earth System Science Data* 13, no. 9: 4349–4383.

Nieto, R., L. Gimeno, L. De la Torre, et al. 2007. "Interannual Variability of Cut-Off Low Systems Over the European Sector: The Role of Blocking and the Northern Hemisphere Circulation Modes." *Meteorology and Atmospheric Physics* 96: 85–101.

Pachauri, R. K., M. R. Allen, V. R. Barros, et al. 2014. "Climate Change 2014: Synthesis Report. Contribution of Working Groups I, II and III to the Fifth Assessment Report of the Intergovernmental Panel on Climate Change." IPCC.

Paranychianakis, N. V., S. Aggelides, and A. N. Angelakis. 2004. "Influence of Rootstock, Irrigation Level and Recycled Water on Growth and Yield of Soultanina Grapevines." *Agricultural Water Management* 69, no. 1: 13–27.

Peixoto, J. P., and A. H. Oort. 1984. "Physics of Climate." *Reviews of Modern Physics* 56: 365–429. https://doi.org/10.1103/RevModPhys.56.365.

Peppler, R. A., and P. J. Lamb. 1989. "Tropospheric Static Stability and Central North American Growing Season Rainfall." *Monthly Weather Review* 117, no. 6: 1156–1180. https://doi.org/10.1175/1520-0493(1989)117<1156:TSSACN>2.0.CO;2.

Pettit, A. N. 1979. "A Non-Parametric Approach to the Change-Point Problem." *Applied Statistics* 28, no. 2: 126–135.

Pinto, P., and M. Belo-Pereira. 2020. "Damaging Convective and Non-Convective Winds in Southwestern Iberia During Windstorm Xola." *Atmosphere* 11, no. 7: 692. https://doi.org/10.3390/atmos11070692.

Prachowski, J., J. Szturc, J. Kučera, and J. Podhrázská. 2024. "Erosion Risk Analysis in a Changing Climate." *Soil and Water Research* 19, no. 1: 50–63. https://doi.org/10.17221/110/2023-SWR.

Prata Gomes, D., M. M. Neves, and E. Moreira. 2016. "An Exploratory Study of Spatial Annual Maximum of Monthly Precipitation in the Northern Region of Portugal." *Physics and Chemistry of the Earth* 94: 77–84. https://doi.org/10.1016/j.pce.2015.12.001.

Ramos, A. M., N. Cortesi, and R. M. Trigo. 2014. "Circulation Weather Types and Spatial Variability of Daily Precipitation in the Iberian Peninsula." *Frontiers in Earth Science* 2: 25.

Ramos, A. M., M. J. Martins, R. Tomé, and R. M. Trigo. 2018. "Extreme Precipitation Events in Summer in the Iberian Peninsula and Its Relationship With Atmospheric Rivers." *Frontiers in Earth Science* 6: 1–10. https://doi.org/10.3389/feart.2018.00110.

Ramos, A. M., R. Ramos, P. Sousa, R. M. Trigo, M. Janeira, and V. Prior. 2011. "Cloud to Ground Lightning Activity Over Portugal and Its Association With Circulation Weather Types." *Atmospheric Research* 101, no. 1: 84–101. https://doi.org/10.1016/j.atmosres.2011.01.014.

Ramos, A. M., R. M. Trigo, and M. L. R. Liberato. 2014. "A Ranking of High-Resolution Daily Precipitation Extreme Events for the Iberian Peninsula." *Atmospheric Science Letters* 15, no. 4: 328–334.

Ramos, A. M., R. M. Trigo, M. L. R. Liberato, and R. Tomé. 2015. "Daily Precipitation Extreme Events in the Iberian Peninsula and Its Association With Atmospheric Rivers." *Journal of Hydrometeorology* 16, no. 2: 579–597. https://doi.org/10.1175/JHM-D-14-0103.1.

Rodrigo, F. S., and R. M. Trigo. 2007. "Trends in Daily Rainfall in the Iberian Peninsula From 1951 to 2002." *International Journal of Climatology* 27, no. 4: 513–529. https://doi.org/10.1002/joc.1409.

Rodriguez-Puebla, C., A. H. Encinas, S. Nieto, and J. Garmendia. 1998. "Spatial and Temporal Patterns of Annual Precipitation Variability Over the Iberian Peninsula." *International Journal of Climatology* 18, no. 3: 299–316. https://doi.org/10.1002/(SICI)1097-0088(19980315)18:3<299::AID-JOC247>3.0.CO;2-L.

Sanderson, M. G., M. Teixeira, N. Fontes, S. Silva, and A. Graça. 2023. "The Probability of Unprecedented High Rainfall in Wine Regions of Northern Portugal." *Climate Services* 30: 100363. https://doi.org/10.1016/j.cliser.2023.100363.

Santos, J. A., C. Andrade, J. Corte-Real, and S. Leite. 2009. "The Role of Large-Scale Eddies in the Occurrence of Winter Precipitation Deficits in Portugal." *International Journal of Climatology* 29, no. 10: 1493–1507. https://doi.org/10.1002/joc.1818.

Santos, J. A., and M. Belo-Pereira. 2019. "A Comprehensive Analysis of Hail Events in Portugal: Climatology and Consistency With Atmospheric Circulation." *International Journal of Climatology* 39, no. 1: 188–205. https://doi.org/10.1002/joc.5794.

Santos, J. A., and M. Belo-Pereira. 2022. "Sub-Hourly Precipitation Extremes in Mainland Portugal and Their Driving Mechanisms." *Climate* 10, no. 2: 28. https://doi.org/10.3390/cli10020028.

Santos, J. A., J. Corte-Real, and S. M. Leite. 2005. "Weather Regimes and Their Connection to the Winter Rainfall in Portugal." *International Journal of Climatology* 25, no. 1: 33–50. https://doi.org/10.1002/joc.1101.

Santos, J. A., J. Corte-Real, U. Ulbrich, and J. Palutikof. 2007. "European Winter Precipitation Extremes and Large-Scale Circulation: A Coupled Model and Its Scenarios." *Theoretical and Applied Climatology* 87, no. 1–4: 85–102. https://doi.org/10.1007/s00704-005-0224-2.

Santos, J. A., H. Fraga, A. C. Malheiro, et al. 2020. "A Review of the Potential Climate Change Impacts and Adaptation Options for European Viticulture." *Applied Sciences* 10, no. 9: 3092. https://doi.org/10.3390/app10093092.

Santos, J. A., J. G. Pinto, and U. Ulbrich. 2009. "On the Development of Strong Ridge Episodes Over the Eastern North Atlantic." *Geophysical Research Letters* 36, no. 17: 1–6. https://doi.org/10.1029/2009GL039086.

Santos, J. A., M. A. Reis, J. Sousa, et al. 2012. "Cloud-To-Ground Lightning in Portugal: Patterns and Dynamical Forcing." *Natural Hazards and Earth System Sciences* 12, no. 3: 639–649. https://doi.org/10.5194/nhess-12-639-2012.

Santos, J. A., T. Woollings, and J. G. Pinto. 2013. "Are the Winters 2010 and 2012 Archetypes Exhibiting Extreme Opposite Behavior of the North Atlantic Jet Stream." *Monthly Weather Review* 141, no. 10: 3626–3640. https://doi.org/10.1175/MWR-D-13-00024.1.

Santos, M., and M. Fragoso. 2013. "Precipitation Variability in Northern Portugal: Data Homogeneity Assessment and Trends in Extreme Precipitation Indices." *Atmospheric Research* 131: 34–45. https://doi.org/10.1016/j.atmosres.2013.04.008.

Santos, M., J. A. Santos, and M. Fragoso. 2015. "Historical Damaging Flood Records for 1871–2011 in Northern Portugal and Underlying Atmospheric Forcings." *Journal of Hydrology* 530: 591–603. https://doi.org/10.1016/j.jhydrol.2015.10.011.

Schulz, W., G. Diendorfer, S. Pedeboy, and D. R. Poelman. 2016. "The European Lightning Location System EUCLID–Part 1: Performance Analysis and Validation." *Natural Hazards and Earth System Sciences* 16, no. 2: 595–605.

Sousa, J. F., M. Fragoso, S. Mendes, J. Corte-Real, and J. A. Santos. 2013. "Statistical-Dynamical Modeling of the Cloud-To-Ground Lightning Activity in Portugal." *Atmospheric Research* 132: 46–64. https://doi.org/10.1016/j.atmosres.2013.04.010.

Straffelini, E., and P. Tarolli. 2023. "Climate Change-Induced Aridity Is Affecting Agriculture in Northeast Italy." *Agricultural Systems* 208: 103647. https://doi.org/10.1016/j.agsy.2023.103647.

Trigo, I. F. 2006. "Climatology and Interannual Variability of Storm-Tracks in the Euro-Atlantic Sector: A Comparison Between ERA-40 and NCEP/NCAR Reanalyses." *Climate Dynamics* 26, no. 2–3: 127–143. https://doi.org/10.1007/s00382-005-0065-9.

Trigo, R. M., and C. C. Da Câmara. 2000. "Circulation Weather Types and Their Influence on the Precipitation Regime in Portugal." *International Journal of Climatology* 20: 1559–1581.

Trigo, R. M., M. A. Valente, I. F. Trigo, et al. 2008. "The Impact of North Atlantic Wind and Cyclone Trends on European Precipitation and Significant Wave Height in the Atlantic." *Annals of the New York Academy of Sciences* 1146, no. 1: 212–234.

Vaisala. 2024a. "Advanced Lightning Sensor LS7002 Vaisala." https://www.vaisala.com/en/systems/lightning/single-point-sensors/advanced-lightning-sensor-ls7002.

Vaisala. 2024b. "Total Lightning Processor." https://www.vaisala.com/en/products/weather-environmental-sensors/total-lightning-processor.

Valero, F., M. L. Martín, M. G. Sotillo, A. Morata, and M. Y. Luna. 2009. "Characterization of the Autumn Iberian Precipitation From Long-Term Datasets: Comparison Between Observed and Hindcasted Data." *International Journal of Climatology: A Journal of the Royal Meteorological* 29, no. 4: 527–541. https://doi.org/10.1002/joc.1726.

Von Neumann, J. 1941. "Distribution of the Ratio of the Mean Square Successive Difference to the Variance." *Annals of Mathematical Statistics* 12, no. 4: 367–395.

Wang, W., A. Pijl, and P. Tarolli. 2022. "Future Climate-Zone Shifts Are Threatening Steep-Slope Agriculture." *Nature Food* 3, no. 3: 193–196. https://doi.org/10.1038/s43016-021-00454-y.

Woollings, T., J. G. Pinto, and J. A. Santos. 2011. "Dynamical Evolution of North Atlantic Ridges and Poleward Jet Stream Displacements." *Journal of the Atmospheric Sciences* 68, no. 5: 954–963. https://doi.org/10.1175/2011JAS3661.1.

Supporting Information

Additional supporting information can be found online in the Supporting Information section.